

COSMOGRAIL XVI: Time delays for the quadruply imaged quasar DES J0408–5354 with high-cadence photometric monitoring

F. Courbin¹, V. Bonvin¹, E. Buckley-Geer², C.D. Fassnacht³, J. Frieman^{2,4}, H. Lin², P.J. Marshall²⁴, S.H. Suyu^{6,7,8}, T. Treu⁹, T. Anguita^{10,11}, V. Motta¹², G. Meylan¹, E. Paic¹, M. Tewes¹³, A. Agnello¹⁴, D.C.-Y. Chao⁶, M. Chijani¹⁰, D. Gilman⁹, K. Rojas¹², P. Williams⁹, A. Hempel¹⁰, S. Kim^{15,16}, R. Lachaume^{15,16}, M. Rabus^{15,16}, T. M. C. Abbott¹⁷, S. Allam², J. Annis², M. Banerji^{18,19}, K. Bechtol²⁰, A. Benoit-Lévy^{21,22,23}, D. Brooks²², D. L. Burke^{24,25}, A. Carnero Rosell^{26,27}, M. Carrasco Kind^{28,29}, J. Carretero³⁰, C. B. D'Andrea³¹, L. N. da Costa^{26,27}, C. Davis²⁴, D. L. DePoy³², S. Desai³³, B. Flaugher², P. Fosalba³⁴, J. García-Bellido³⁵, E. Gaztanaga³⁴, D. A. Goldstein^{36,37}, D. Gruen^{24,25}, R. A. Gruendl^{28,29}, J. Gschwend^{26,27}, G. Gutierrez², K. Honscheid^{38,39}, D. J. James^{40,17}, K. Kuehn⁴¹, S. Kuhlmann⁴², N. Kuropatkin², O. Lahav²², M. Lima^{43,26}, M. A. G. Maia^{26,27}, M. March³¹, J. L. Marshall³², R. G. McMahon^{18,19}, F. Menanteau^{28,29}, R. Miquel^{44,30}, B. Nord², A. A. Plazas⁴⁵, E. Sanchez⁴⁶, V. Scarpine², R. Schindler²⁵, M. Schubnell⁴⁷, I. Sevilla-Noarbe⁴⁶, M. Smith⁴⁸, M. Soares-Santos², F. Sobreira^{49,26}, E. Suchyta⁵⁰, G. Tarle⁴⁷, D. L. Tucker², A. R. Walker¹⁷, and W. Wester²

(Affiliations can be found after the references)

November 3, 2021

ABSTRACT

We present time-delay measurements for the new quadruple imaged quasar DES J0408–5354, the first quadruple imaged quasar found in the Dark Energy Survey (DES). Our result is made possible by implementing a new observational strategy using almost daily observations with the MPIA 2.2m telescope at La Silla observatory and deep exposures reaching a signal-to-noise ratio of about 1000 per quasar image. This data quality allows us to catch small photometric variations (a few mmag rms) of the quasar, acting on temporal scales much shorter than microlensing, hence making the time delay measurement very robust against microlensing. In only 7 months we measure very accurately one of the time delays in DES J0408–5354: $\Delta t(AB) = -112.1 \pm 2.1$ days (1.8%) using only the MPIA 2.2m data. In combination with data taken with the 1.2m Euler Swiss telescope, we also measure two delays involving the D component of the system $\Delta t(AD) = -155.5 \pm 12.8$ days (8.2%) and $\Delta t(BD) = -42.4 \pm 17.6$ days (41%), where all the error bars include systematics. Turning these time delays into cosmological constraints will require deep HST imaging or ground-based Adaptive Optics (AO), and information on the velocity field of the lensing galaxy.

Key words. methods: data analysis – gravitational lensing: strong – cosmological parameters

1. Introduction

Accurate and precise measurements of the time delay(s) between the multiple images of gravitationally lensed quasars offer an independent way of constraining cosmology. The method is simple and is mostly sensitive to H_0 with weak dependence on other cosmological parameters (Refsdal 1964). For this reason, the time-delay method has the potential to alleviate the degeneracies between cosmological parameters other than H_0 . In addition, it provides helpful input to resolve the tension between H_0 as measured by Planck assuming a flat Λ CDM model (Planck Collaboration et al. 2016) and the local distance ladder, i.e. Cepheid stars (Freedman 2017; Freedman et al. 2001) and type Ia supernovae (e.g. Riess et al. 2016). Quasar time delays offer an opportunity to measure H_0 completely independently of any of the above probes.

The method requires several ingredients: i) time-delay measurements, ii) models constraining the mass and light distribution in the lensing galaxy, iii) an estimate of the contribution of objects along the line of sight to the overall potential well. The first point has been addressed by the COSMOGRAIL program, started in 2004 and delivering since then some of the best-quality time-delay measurements (e.g. Bonvin et al. 2017; Rathna Kumar et al. 2013; Tewes et al. 2013b; Courbin et al.

2011; Vuissoz et al. 2008; Courbin et al. 2005; Eigenbrod et al. 2005). In parallel, detailed modeling techniques have been developed and used on deep Hubble Space Telescope (HST) images in combination with spectroscopic data providing crucial constraints on the dynamics of the lensing galaxy (Treu & Koopmans 2002; Suyu et al. 2006, 2009). Such models, in combination with an estimate of the overall mass along the line-of-sight (e.g. Hilbert et al. 2009; McCully et al. 2017, 2014; Collett et al. 2013) allow one to measure the time-delay distance and consequently the Hubble parameter, H_0 (e.g. Suyu et al. 2010).

In order to perform precise cosmological measurement with strongly lensed quasars, these three ingredients must be accurately constrained. This has become possible only recently, with the joint efforts of the COSMOGRAIL (e.g. Courbin et al. 2005) and H0LiCOW programs (H_0 Lenses in COSMOGRAIL's Wellspring; Suyu et al. 2017), focusing on 5 well selected bright lensed quasars. Recent results can be found in Bonvin et al. (2017); Wong et al. (2017); Rusu et al. (2017); Sluse et al. (2016) who infer $H_0 = 71.9^{+2.4}_{-3.0}$ km s⁻¹Mpc⁻¹ from 3 of the H0LiCOW lenses in a flat Λ CDM universe.

The H0LiCOW sample currently under study includes 5 lenses, with an expected H_0 measurement to <3.5% including systematics (Suyu et al. 2017). Going beyond this will require

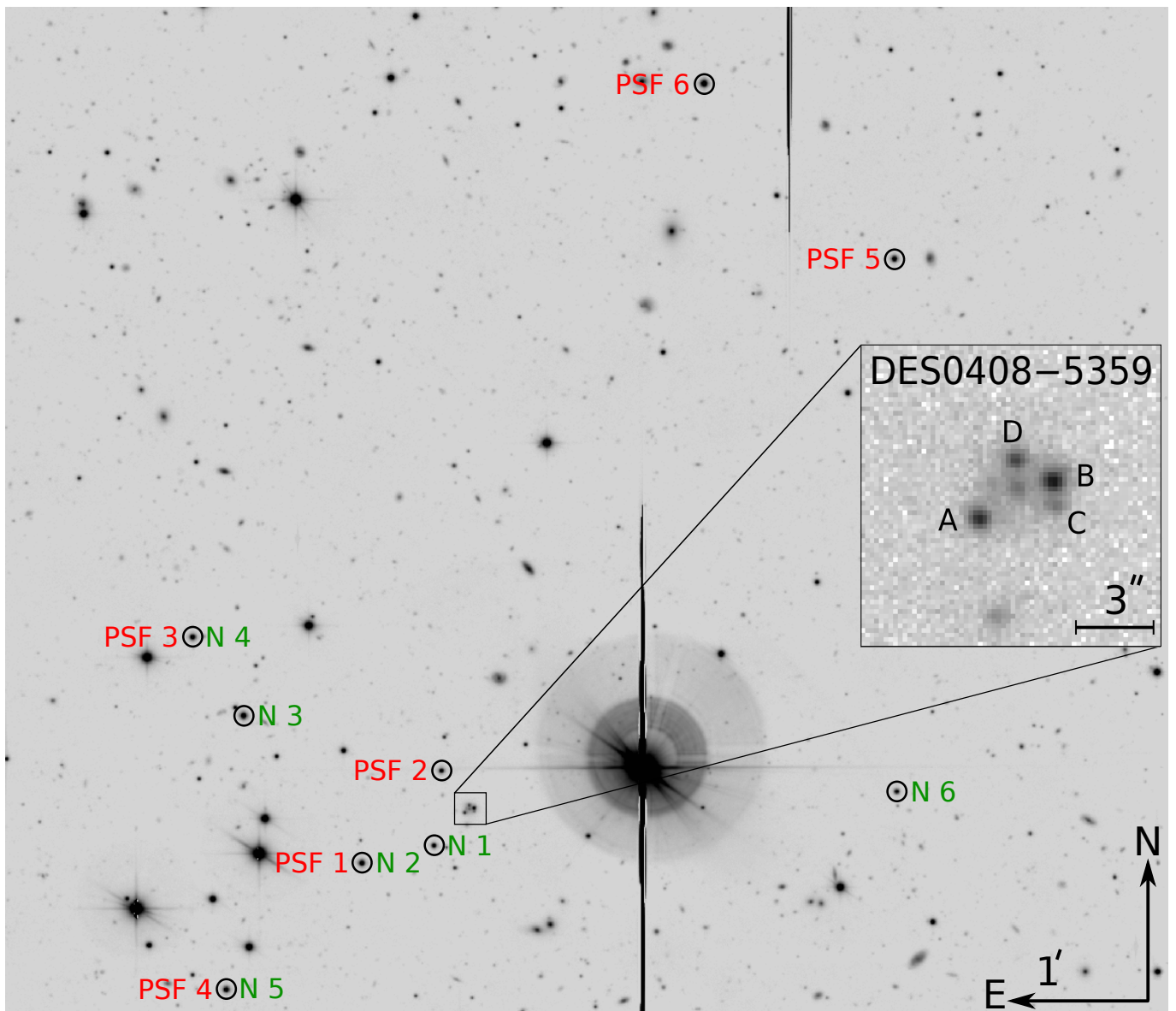


Fig. 1. Part of the field of view around DES J0408–5354 as seen with the 2.2m MPIA/ESO telescope at La Silla observatory. The image is a stack of 150 frames totaling 25h of exposure. The 6 PSF stars used to obtain the photometric light curves with deconvolution photometry are indicated in red. The 6 stars used for the frame-to-frame calibration of the relative photometry are indicated in green. The inset shows a 10'' zoom on DES J0408–5354 and is extracted from a single 640 sec exposure with 0.6'' seeing with the same labeling for the quasar images as in Fig. 1 of Lin et al. (2017). Note that image C is blended with a foreground lensing galaxy labeled G2 in Agnello et al. (2017) and Lin et al. (2017).

mass production of time delays. With 55 new time delays and dynamical measurements for the lensing galaxy Jee et al. (2015) estimate that H_0 can be measured to close to 1%. An independent study by Shajib, Agnello & Treu (2017, in prep.) show that with resolved kinematics of the lens (e.g. with JWST or ground-based AO) 1% accuracy on H_0 can be reached with 40 lenses. This requires the discovery of new lenses, which is underway in the Dark Energy Survey (DES) (Ostrovski et al. 2017; Lin et al. 2017; Agnello et al. 2015), deep spectroscopy, the characterisation of the line-of-sight matter distribution, and the measurement of the time delays to a few percents for each individual system. The latter is the goal of the present work.

Because the slow intrinsic variations of the quasar occur roughly at the same time scale as the extrinsic variations (i.e. microlensing), measuring time delays requires years of monitoring.

As the future of time delay cosmography resides in the measurement of several tens of new time delays, each time delay must be measured shortly after the start of the monitoring campaign, i.e. much faster than the typical 10 years it takes with current lens monitoring data. Current lens monitoring campaigns, including COSMOGRAIL, use 1m-class telescopes with a monitoring cadence of about 1 epoch per 3-4 days. The typical photometric accuracy with such data is limited to about 0.01 mag rms for many targets, hence allowing to catch only the most prominent features of the quasar variations. It is difficult, and sometimes impossible, to sufficiently disentangle these from extrinsic variations related to microlensing unless very long light curves are available (e.g. Bonvin et al. 2016; Liao et al. 2015).

In the present work, we implement a new high-cadence and high-signal-to-noise (high-S/N) lens monitoring program, with

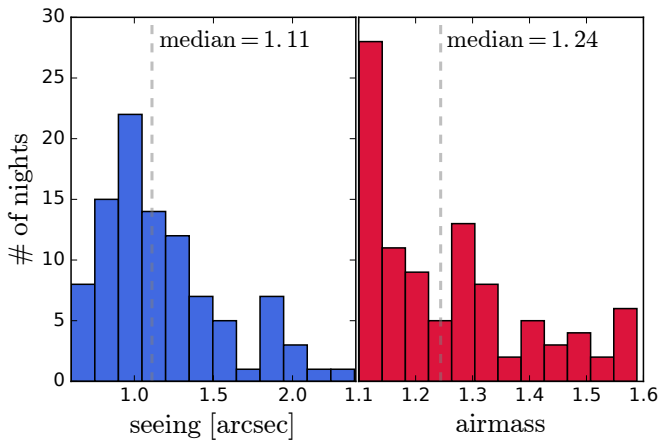


Fig. 2. Seeing and airmass distributions for the 7 months of observations of DES J0408–5354 with the WFI instrument on the MPIA 2.2m telescope.

the goal of measuring time delays in only 1 single observing season. With on average one observing point per day and a S/N of the order of 1000 per quasar component, we can now catch much faster variability in the intrinsic light curve of the quasar (e.g. Mosquera & Kochanek 2011). In almost all cases, these features on time scales of a few days to a few weeks are more than an order of magnitude faster than the extrinsic variations. This difference in signal frequencies makes it possible to disentangle much better between extrinsic and intrinsic quasar variations. As the small and fast quasar variations are frequent (see, e.g. the Kepler data for AGNs in Mushotzky et al. 2011), only a short monitoring period is required to measure time delays, i.e. catching significant quasar variations is guaranteed in a 1-year period provided high S/N and high-cadence data are available. This achieved by using the MPIA 2.2m telescope and the Wide Field Imager (WFI) at ESO La Silla Observatory daily, through a dedicated monitoring program.

We present here our first time delay measurement obtained with the MPIA 2.2m telescope, for the quadruply-imaged quasar DES J0408–5354, at $z_q = 2.375$. DES J0408–5354 was identified as a quadruple imaged quasar by Lin et al. (2017). The lensing galaxy has a redshift of $z_l = 0.597$, measured by (Lin et al. 2017) using the Gemini-South telescope. Agnello et al. (2017) provide simple models for DES J0408–5354 using a deep image of the lens obtained from WFI data and predict time delays for a Λ CDM cosmology and different mass distributions including potential companions to the lensing galaxy, which influence the time-delay predictions.

2. Observations and photometry

The observational material for the present time-delay measurement consists of almost daily imaging data with the MPIA 2.2m telescope and of bi-weekly imaging with the 1.2m Euler Swiss telescope, both at ESO La Silla.

We started the observations on 1 October 2016 with the MPIA 2.2m telescope at ESO La Silla to monitor DES J0408–5354 through the R_c filter. The WFI instrument, mounted in the 2.2m telescope, has a total field of view of $36' \times 36'$, covered by 8 CCDs with a pixel size of $0.2''$. For our monitoring purpose we use only 1 chip to ensure a stable night-to-night calibration. This chip has a field of view of $9' \times 18'$. Part of this it is shown in Fig. 1.

The WFI was used almost daily until 8 April 2017, i.e. over a total of 7 months of visibility of the object, except for 14 consecutive nights between 10 December 2016 and 24 December 2016 due to technical problems and for 1 week in January 2017 due to an extended period of poor weather. For each observing epoch, 4 dithered exposures of 640 sec each were taken in the R_c filter. A total of 459 images were taken in 7 months, of which we use 398 which have adequate seeing and PSF quality. More precisely, we removed the images with 1- a seeing above $3.0''$, 2- a mean ellipticity above $e = 0.4$, 3- a sky level about 10000 electrons, 4- obvious failure in the PSF modeling. On average, the resulting temporal sampling was one observing point every 1.96 day. The median seeing over this period was $1.1''$. Thanks to the flexible scheduling of the observations at the telescope it was possible to observe DES J0408–5354 most of the time at low airmass. The seeing and airmass distributions of the observations are given in Fig. 2.

The high-cadence and high-S/N (2-3 mmag rms per quasar image) obtained with the 2.2m telescope allow us to catch much smaller and much shorter photometric variations than the COSMOGRAIL observations obtained with smaller 1m-size telescopes. We can typically see signals as small as a few mmags and as short as a 15-20 days, which is crucial to avoid contamination by extrinsic variations, as illustrated in Sect. 3

The data from the 1.2m Euler telescope were obtained in the R -band with the ECAM instrument from July 2016 to April 2017. The pixel size of the camera is $0.238''$, providing a field of view of $14'$ on-a-side. We took, for each of the 45 observing epochs 6 exposures of 360 sec each, i.e. 36 min in total. The mean temporal sampling for the Euler observations is of only 1 point every 5 days, but the Euler observations started about 100 days before the WFI observations, hence extending the length of the light curves.

The data reduction procedure applied to the images follows the standard COSMOGRAIL pipeline, as applied to the data obtained with the 1.2m Euler telescope for RX J1131–123 (Tewes et al. 2013b) and HE 0435–1223 (Bonvin et al. 2017). It includes subtraction of a bias level and flat-fielding using sky flats taken on average every few nights. Each frame is then sky-subtracted using the GLOBAL option in the SExtractor package (Bertin & Arnouts 1996). The data from the 2.2m telescope have significant fringe patterns on bright nights. We therefore construct a fringe image by iteratively sigma-clipping the four dithered exposure of each night and by taking the median. This image is then subtracted from the individual dithered exposures taken each night which are subsequently registered to the same pixel grid.

We carry out the photometric measurements using the deconvolution photometry with the so-called MCS image deconvolution algorithm (Magain et al. 1998; Cantale et al. 2016). This algorithm first computes a deconvolution kernel from the images of stars. The kernel is chosen so that the Point Spread Function (PSF) in the deconvolved images is a circular Gaussian function with a Full-Width-Half-Maximum (FWHM) of 2 pixels. The pixel size in the deconvolved images is half that of the original data, i.e. the resolution in the resulting images is $0.2''$ for WFI and the pixel size is $0.1''$. We show in Fig. 1 the PSF stars used as well as the reference stars for the image-to-image flux calibration.

The MCS algorithm deconvolves all the registered images simultaneously, i.e. each one with its own PSF. However all images share the same deconvolved model, which is decomposed into a point-source channel (quasar images) and an extended-channel (lensing galaxy and faint quasar host galaxy). In this

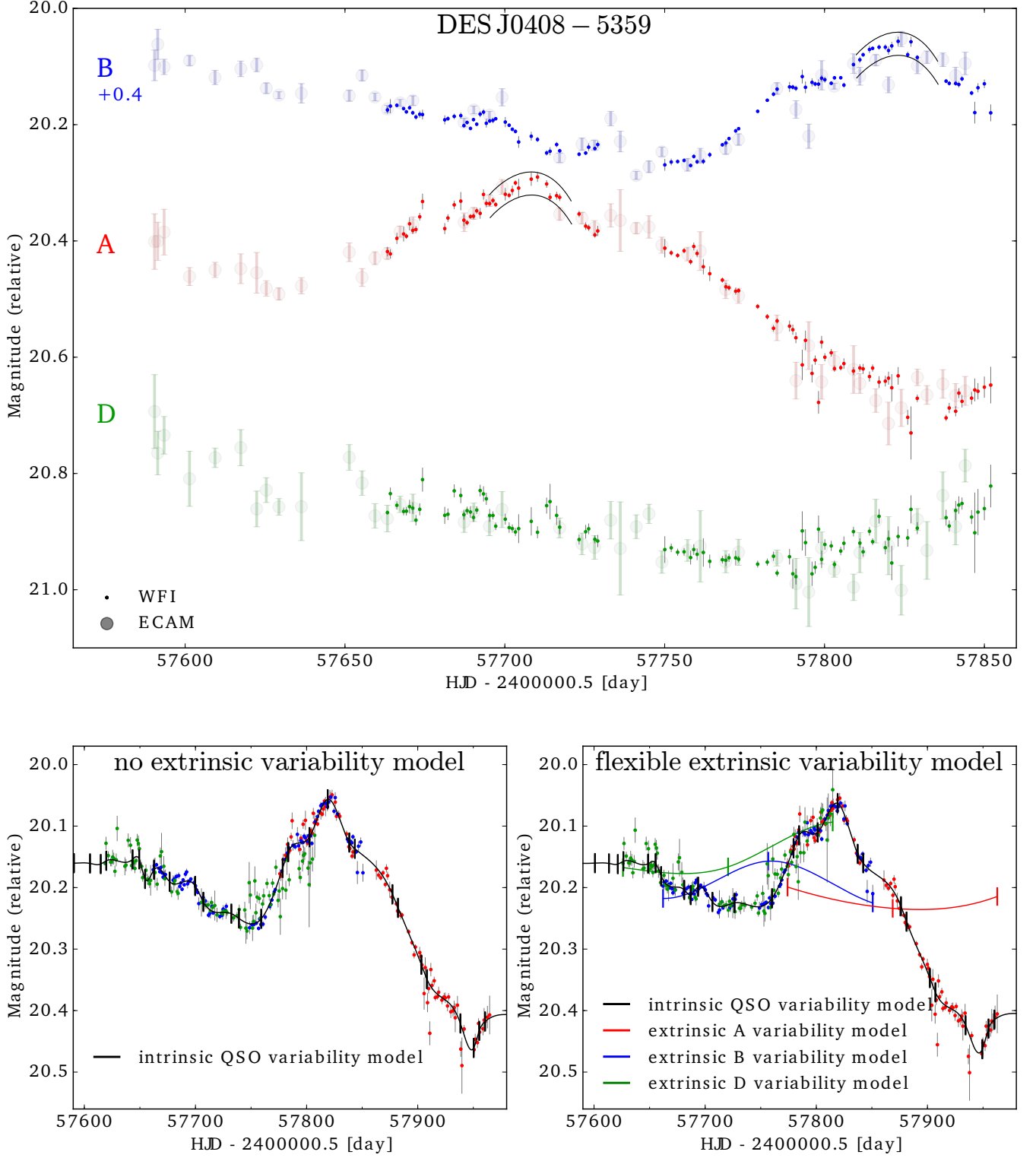


Fig. 3. *Top:* light curves for DES J0408–5354 obtained in the R_c filter with the MPIA 2.2m telescope and the WFI instrument. The points obtained with the 1.2m Euler telescope are also shown, with larger and thicker symbols. To guide the eye, the structure constraining the most the AB time delay is indicated between black solid lines. *Bottom left:* spline-fitting of the intrinsic quasar variations (with an initial knot step of $\eta = 15$ days) and time delay determination when neglecting extrinsic variation due to microlensing. Note that the time delay values do not depend much on the choice of this η parameter which is only an initial value optimized during the fit. *Bottom right:* same as bottom left but now including extrinsic variations (color curves). For more clarity the lower S/N Euler data are shown only in the upper left panel. Our light curves are available online at CDS and on cosmogra1.org.

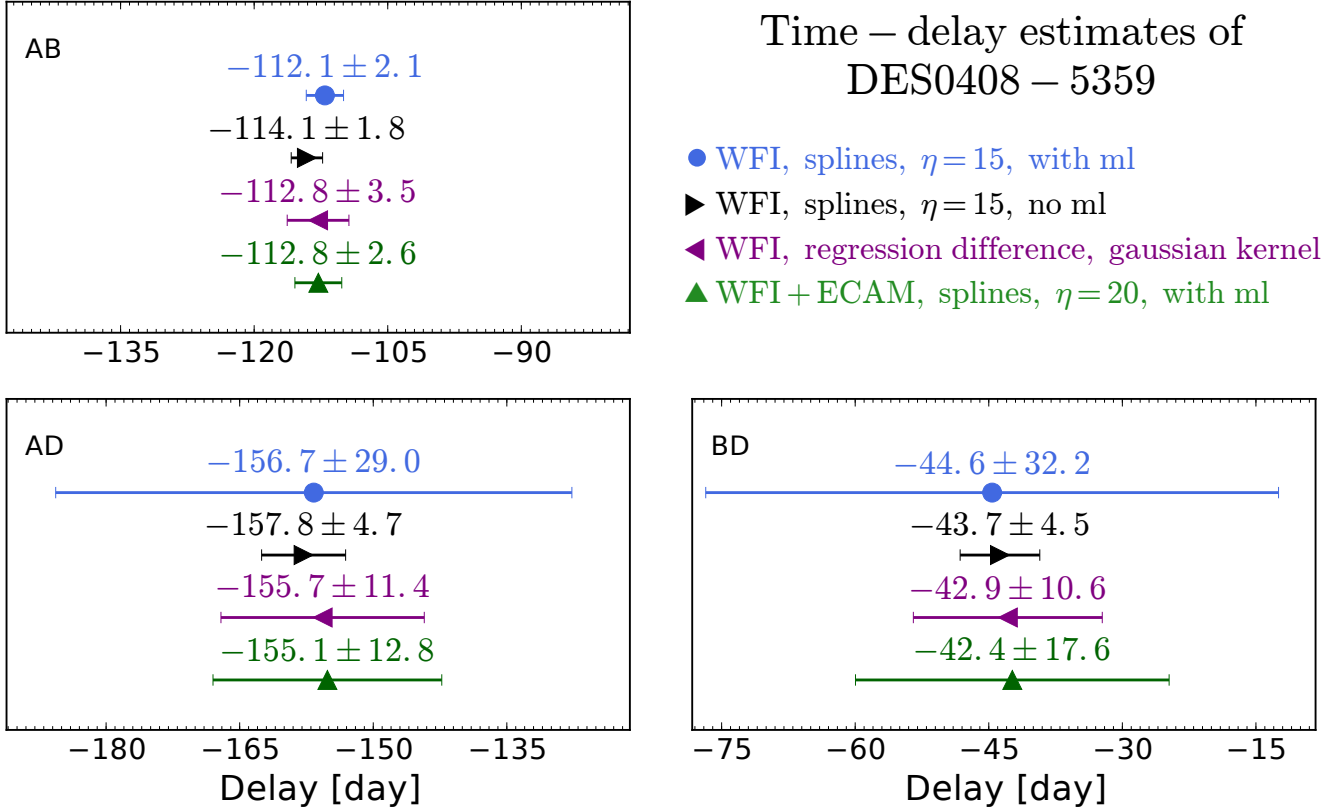


Fig. 4. Time delay measurements for the 3 brightest quasar images of DES J0408–5354 using the data shown in Fig. 3. The time delay measurements are carried out in 3 different ways. In blue are shown the results using only the WFI data and the spline fitting method and in purple with the regdiff method. In green are shown the results for the combined WFI+Euler data set using the spline fitting method. For comparison we also show, in black, the spline fitting result when using only the high-cadence WFI data and no model for the microlensing extrinsic variations. A negative $\Delta t(AB)$ means that signal from image A reaches the observer’s plane before B.

process, the position of the point sources is the same for all images as well as the extended-channel but the intensities of the point sources vary from image to image, hence leading to the photometric light curves. The latter are presented for the three brightest lensed images of DES J0408–5354 in Fig. 3 which shows the striking difference in depth and sampling between the 2.2m data and the Euler ones. Yet, the two data sets agree and complement each other well and exhibit fine structures in the light curves of A and B. The D component, however, has much shallower variations given the larger photometric error bars and will need further monitoring.

3. Time delay measurement

We use PyCS¹, a toolbox containing several algorithms to measure time delays from quasar light curves and accounting for the intrinsic variations (from the lensed source) and extrinsic variations (microlensing) in the data. The (public) algorithm was proposed by Tewes et al. (2013a) and tested on simulated data from the Time Delay Challenge (Bonvin et al. 2016; Liao et al. 2015), with overall excellent performances.

3.1. Time delay measurement with PyCS

PyCS is the standard curve-shifting toolbox of the COSMOGRAIL project. We apply it to the WFI light curves

as well as on the combination of the Euler and WFI data. We do not attempt to measure a time delay using the Euler data on their own as they contain only 45 epochs over the duration of the observations. However, used in combination with the WFI images, they increase the time baseline with observations between July 2016 and October 2016.

We use the two best algorithms of the PyCS toolbox: the *free-knot spline* technique and the *regression difference* technique (Tewes et al. 2013a). In the former, the intrinsic and extrinsic variations in the light curves are modeled explicitly as spline functions. In doing so, we give more flexibility to the spline representing the intrinsic variations of the quasar than to the spline representing extrinsic variations. This flexibility is varied through a parameter η representing the initial knot spacing in the splines (Tewes et al. 2013a). The value of η is optimized using simulated light curves that mimic the properties of the data. These simulated light curves are produced using the same toolbox as in Sect. 3.2. Note, however, that our results depend little on the exact value for η and that for a fixed choice of η the position of the knots can change during the fit. This avoids many of the traditional “oscillation” problems with spline fit using fixed (and possibly badly placed) knots. To fit the present data, we use splines with only 3 knots to represent the microlensing. We further impose that the central knot stays centered on the temporal axis between the light curve extrema during the minimization process. Adding knots to the microlensing splines does not change significantly the results.

¹ PyCS can be obtained from <http://www.cosmograil.org>

In the *regression difference* technique, we minimize the variability of the difference between Gaussian-process regressions performed on each light curve individually. This second method has no explicitly parametrized form for the extrinsic variability, which makes the two techniques fundamentally different and independent. We apply the two methods to our data in the same way as in Bonvin et al. (2017) and Tewes et al. (2013a), who also give the procedure to derive the random and systematic errors from simulated light curves. As the results may depend on some of the key parameters that characterize each method, we perform robustness checks identical to the ones in Bonvin et al. (2017); we use PyCS with a large range of method parameters, namely the number of knots of the spline technique and the covariance function of the *regression difference* technique (see Tewes et al. 2013a, for a full description of these parameters). We do not find significant differences in the mean time-delay values among the results obtained for the various tests, although the precision might vary.

The time-delay measurements are summarized in Fig. 4 for different data sets, i.e. with and without the Euler data. We note that the longer-baseline Euler data improve the time-delay estimates involving the D image when used in combination with the 2.2m WFI data. The latter have strong constraining power as high-frequency structures are captured in the curves, i.e. mostly the A and B components which display two strong features, including two inflection points in the case of B. For the much fainter D image, the situation is more complex as it displays only one shallow inflection point and no clear feature that can be matched to the other light curves.

3.2. Error estimates

In PyCS, the error estimates are done by running the curve-shifting techniques on mock light curves created from a generative model (see Tewes et al. 2013a). In these mocks, the intrinsic and extrinsic variations of the quasar are the same as the one inferred from the real data as well as the temporal sampling and photometric errors. What changes from mock to mock are the correlated extrinsic variability (whose statistical properties mimic the observations), the photometric noise, the true time delays and the value of the simulated data points. The mock curves are drawn so that they have the same “time-delay constraining power” than the original data, i.e. the properties of the residuals after fitting the mock with a spline are statistically the same as on the real data.

We carry out simulations for a broad range of true input time delays around the measured value. This error analysis is summarized in Fig. 5 which, for each of the true time delay tested, provides the random and systematic errors. The final error for the delay is taken as the worst random error over all the bins, combined in quadrature with the worst systematic error. Obviously, the size of the bins, as well as the range of true time-delays explored when drawing the simulated light curves can have an impact on the final error. Part of the robustness checks we performed are intended to ensure that we do not overestimate or underestimate the errors by choosing inappropriate bin sizes and ranges in true time-delays. In the present case, our choice of possible true time-delays ranges up to ± 10 days from our initial estimation obtained by running our point estimator on the original data. Such a wide range encompasses our uncertainty regarding the time delays of DES J0408–5354 that have never been measured before, yet is also small enough to make sure that simulated light curves (especially A and D) are sufficiently overlapping. We can note from the bottom panels of Fig. 5, that

the large systematic errors of the spline optimizer (in blue and green) come mostly from the simulations with extreme values of true delays.

We note that for the A and B light curves, which benefit from high-S/N data, the time delay is very accurate, whatever true delay is tested. This illustrates the importance of catching as many faint and short-duration structures in the light curves and the impact of high-cadence and high-S/N data. As a robustness test, we carry out the time-delay measurements without modeling explicitly extrinsic variations when using the spline technique. These results are indicated in black in Figs. 4 & 5 and show that the value of the time delays do not depend much on the extrinsic variations for the AB delay. Future observations of other objects will show if this is specific to DES J0408–5354 or a more general behaviour of the results with high-cadence and high-S/N light curves. Our final time delay value for AB is $\Delta t(AB) = -112.1 \pm 2.1$ days (1.8%), as obtained with the *free-knot spline* method using only the WFI data and extrinsic variations explicitly included. We make this choice because the time-delay measurement is precisely determined mostly thanks to the finely modeled peak in the WFI light curves (around mjd = 57710 in A and 57820 in B). This peak is only crudely visible in the Euler data. Thus, adding the latter data set in the present case would only increase the overall noise. We also note that including extrinsic variations explicitly only slightly shifts the result while keeping the precision unchanged, as shown in Fig. 4. We chose nevertheless to explicitly include extrinsic variations since the residuals in the data speak in favor of it and since it is physically motivated: microlensing and the subsequent extrinsic variations is present at some level in almost every lensed quasar known to date (Mosquera & Kochanek 2011).

In contrast to AB, the precision on the AD and BD delays depends on how extrinsic variations are modeled. Due to the lack of fine and sharp structures in the D light curve, and with only one shallow inflection point, the intrinsic and extrinsic variations are almost fully degenerate. We choose as our final results for these two delays the values obtained with the *free-knot spline* techniques for the combined Euler and WFI data sets. These times delay estimates are $\Delta t(AD) = -155.5 \pm 12.8$ days (8.2%) and $\Delta t(BD) = -42.4 \pm 17.6$ days (41%).

Finally, it is worth noting that the delays obtained with the *regression difference* technique applied only to WFI are consistent with the ones from the *free-knot spline* techniques, and the AD and BD delays are even more precisely measured. We however prefer to stick to the results of the *free-knot splines* since they are much more precise for AB, which is currently - and by far - the most constraining delay to be used in future modeling of this lensed system. We also explicitly avoid cherry-picking the best technique per delay, i.e. in the present case the *free-knot splines* for AB and the *regression difference* for AD and BD. Such an ad’hoc choice may introduce a bias difficult to quantify. Finally, the *free-knot splines* technique is the one giving the smallest systematics according to Fig. 5.

3.3. Comparison with simple models

Simple lens models are provided by Agnello et al. (2017) and are useful to design the monitoring strategy. They show that DES J0408–5354 is challenging in terms of measuring time delays, as the longest one is half the visibility window of the object. Even under these difficult conditions, the MPIA 2.2m data allow us to measure it to 1.8% accuracy and precision, by unveiling short and small photometric variations of the quasar images A and B.

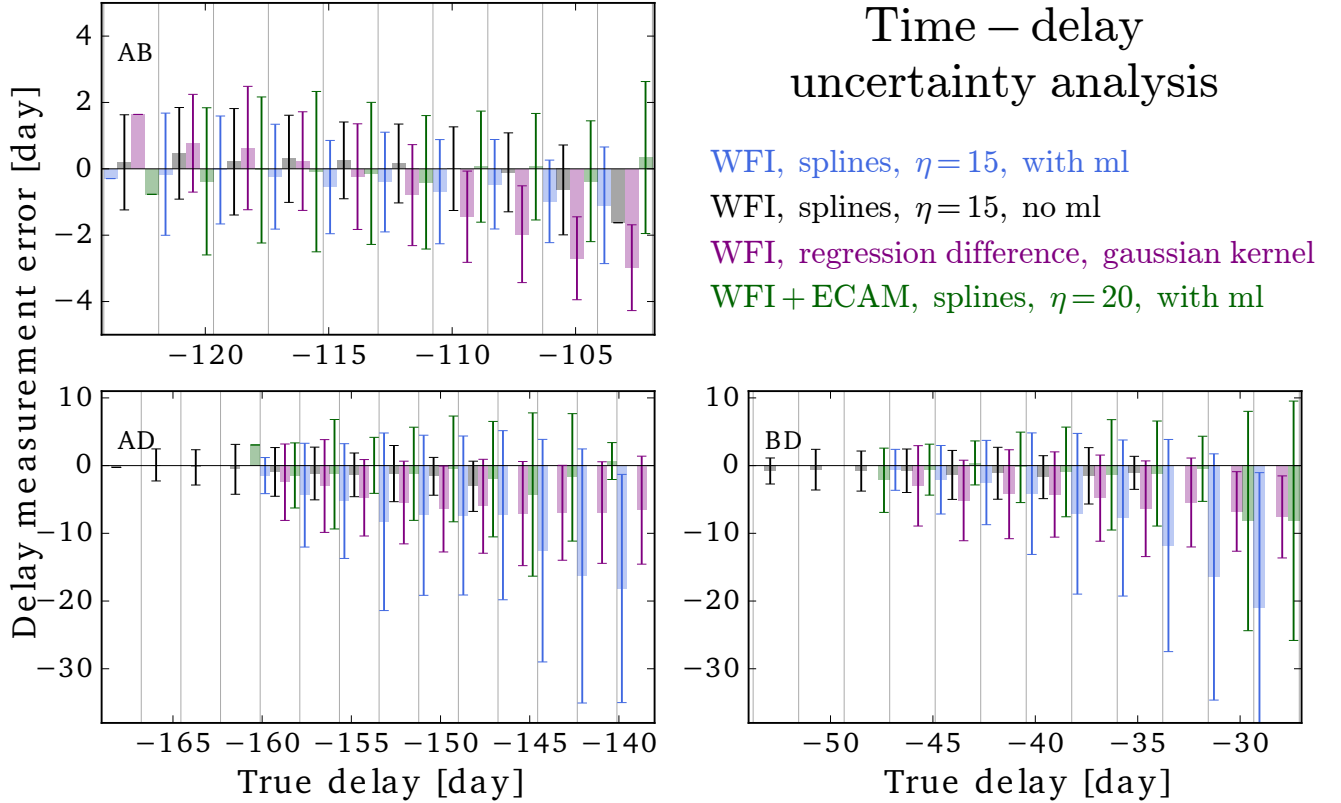


Fig. 5. Error estimates for the time-delay measurements performed on 1000 simulated light curves. The color code is the same as in Fig. 4. The x -axis of each panel shows the values for the true time-delay in the mock light curves. For each time-delay value are shown the random error bars as thin lines and the systematic errors as thick lines. The values for the time delays, as measured on the real data correspond to the center of each panel.

The time delay we find for AB is in marginal agreement with the predictions of Agnello et al. (2017) but a detailed comparison between our measurement and the model predictions for DES J0408–5354 would be hazardous at this stage. Indeed, two values of the delay are possible as quasar image C has a possible companion in its vicinity. The predicted delays are $\Delta t(AB) \sim -85$ days for a model with a companion and $\Delta t(AB) \sim -125$ days for a model without a companion galaxy, which introduces degeneracies in the models that cannot be lifted with the current imaging data, which only provide the relative positions of the quasar images relative to the lensing galaxy. Until deep HST or ground-based AO images are available it will be impossible to discriminate between models with or without this companion object.

Independently of the characterization of the companion, the minimum information required to constrain lens models, even with few degrees of freedom, are 1- sharp images of the lensed quasar host galaxy and 2- dynamics of the main lensing galaxy, as is used for all objects in the H0LiCOW program (Suyu et al. 2017; Bonvin et al. 2017). Suyu et al. (2014) illustrate how a radially thick Einstein ring can lift most model degeneracies, in combination with the central velocity dispersion of the lens. Acquisition of both HST images of the Einstein ring and spectra of the lens are under way.

4. Conclusion

We demonstrate a new observational strategy for measuring time delays in lensed quasars, using high-cadence and high signal-to-

noise monitoring photometry. The data, obtained almost daily over 7 months with the MPIA 2.2m telescope at ESO La Silla allow us to measure $\Delta t(AB) = -112.1 \pm 2.1$ days (1.8%), $\Delta t(AD) = -155.5 \pm 12.8$ days (8.2%) and $\Delta t(BD) = -42.4 \pm 17.6$ days (41%), where the error bars include systematics due to residual extrinsic variations. For the AB time delay, we note that the time-delay values depend little on the way extrinsic variations are modeled, hence indicating that the high-frequency signal in the light curves from the WFI instrument on the 2.2m telescope is dominated by the intrinsic variations of the quasar, as expected. For the D component, however, we only report a tentative delay due to the lack of fast variations seen in the light curve of this faint lensed image.

With the current imaging data for DES J0408–5354 it is too early to compare in detail the model predictions for the time delays (Agnello et al. 2017) and our measurements. Imaging with the HST or with ground-based adaptive optics (AO) is mandatory before drawing any conclusions and before doing any cosmological inference with DES J0408–5354. Fortunately, the object has several bright stars in its immediate vicinity, making it an excellent prey for VLT and AO, e.g. with the MUSE integral field spectrograph, providing the required dynamical information on the lensing galaxy(ies). In the near-IR observations with the VLT and the Hawk-I imager and the GRAAL AO system would both allow to measure the dynamics of the lens and probe the mass along the line of sight on a $7' \times 7'$ field of view.

With the many wide-field surveys taking place at the moment (DES, KiDS, CFIS, DECaLS, HSC) and with LSST and Euclid coming in a fairly near future, the available number of

lensed quasars will increase dramatically (e.g. Oguri & Marshall 2010). We show how daily and very high signal-to-noise observations during 1 single season can match and potentially surpass long-term monitoring carried out at a lower rate (e.g. weekly) over many years. This should be accounted for when planning synoptic surveys such as the LSST. Although the latter will definitely yield very high signal-to-noise images, the full benefit of monitoring data with a 8m telescope will be much enhanced in combination with a daily cadence or very close to a daily cadence.

We are currently monitoring 4 objects since October 2016 with the MPIA 2.2m. From a preliminary analysis of these 4 targets, we anticipate that reliable (i.e. to a few percents) time delays will be measured for 3 of them. We show here our results for DES J0408–5354, for which the observing season is finished.

Acknowledgements. The authors would like to thank R. Gredel for his help in setting up the program at the MPIA 2.2m telescope. This work is supported by the Swiss National Science Foundation (SNSF). S.H. Suyu and D.C.Y. Chao thank the Max Planck Society for support through the Max Planck Research Group for SHS. T. Treu acknowledges support by the National Science Foundation through grant 1450141, by the Packard Foundation through a Packard Research Fellowship and by the UCLA Dean of Physical Sciences. K.Rojas is supported by Becas de Doctorado Nacional CONICYT 2017. T. Anguita and M. Chijani acknowledge support by proyecto FONDECYT 11130630 and by the Ministry for the Economy, Development, and Tourism Programa Inicativa Científica Milenio through grant IC 12009, awarded to The Millennium Institute of Astrophysics (MAS). M. Tewes acknowledges support from the DFG grant Hi 1495/2-1. J. Garcia-Bellido is supported by the Research Project FPA2015-68048 [MINECO-FEDER], and the Centro de Excelencia Severo Ochoa Program SEV-2012-0249. C.D. Fassnacht acknowledges support from the National Science Foundation grant AST-1312329 and from the UC Davis Physics Department and Dean of Math and Physical Sciences.

Funding for the DES Projects has been provided by the U.S. Department of Energy, the U.S. National Science Foundation, the Ministry of Science and Education of Spain, the Science and Technology Facilities Council of the United Kingdom, the Higher Education Funding Council for England, the National Center for Supercomputing Applications at the University of Illinois at Urbana-Champaign, the Kavli Institute of Cosmological Physics at the University of Chicago, the Center for Cosmology and Astro-Particle Physics at the Ohio State University, the Mitchell Institute for Fundamental Physics and Astronomy at Texas A&M University, Financiadora de Estudos e Projetos, Fundação Carlos Chagas Filho de Amparo à Pesquisa do Estado do Rio de Janeiro, Conselho Nacional de Desenvolvimento Científico e Tecnológico and the Ministério da Ciência, Tecnologia e Inovação, the Deutsche Forschungsgemeinschaft and the Collaborating Institutions in the Dark Energy Survey.

The Collaborating Institutions are Argonne National Laboratory, the University of California at Santa Cruz, the University of Cambridge, Centro de Investigaciones Energéticas, Medioambientales y Tecnológicas-Madrid, the University of Chicago, University College London, the DES-Brazil Consortium, the University of Edinburgh, the Eidgenössische Technische Hochschule (ETH) Zürich, Fermi National Accelerator Laboratory, the University of Illinois at Urbana-Champaign, the Institut de Ciències de l’Espai (IEEC/CSIC), the Institut de Física d’Altes Energies, Lawrence Berkeley National Laboratory, the Ludwig-Maximilians Universität München and the associated Excellence Cluster Universe, the University of Michigan, the National Optical Astronomy Observatory, the University of Nottingham, The Ohio State University, the University of Pennsylvania, the University of Portsmouth, SLAC National Accelerator Laboratory, Stanford University, the University of Sussex, Texas A&M University, and the OzDES Membership Consortium.

The DES data management system is supported by the National Science Foundation under Grant Number AST-1138766. The DES participants from Spanish institutions are partially supported by MINECO under grants AYA2015-71825, ESP2015-88861, FPA2015-68048, SEV-2012-0234, SEV-2012-0249, and MDM-2015-0509, some of which include ERDF funds from the European Union. IFAE is partially funded by the CERCA program of the Generalitat de Catalunya.

References

Agnello, A., Lin, H., Buckley-Geer, L., et al. 2017, ArXiv1702.00406
 Agnello, A., Treu, T., Ostrovski, F., et al. 2015, MNRAS, 454, 1260
 Bertin, E. & Arnouts, S. 1996, A&AS, 117, 393
 Bonvin, V., Courbin, F., Suyu, S. H., et al. 2017, MNRAS, 465, 4914

Bonvin, V., Tewes, M., Courbin, F., et al. 2016, A&A, 585, A88
 Cantale, N., Courbin, F., Tewes, M., Jablonka, P., & Meylan, G. 2016, A&A, 589, A81
 Collett, T. E., Marshall, P. J., Auger, M. W., et al. 2013, MNRAS, 432, 679
 Courbin, F., Chantry, V., Revaz, Y., et al. 2011, A&A, 536, A53
 Courbin, F., Eigenbrod, A., Vuissoz, C., Meylan, G., & Magain, P. 2005, in IAU Symposium, Vol. 225, Gravitational Lensing Impact on Cosmology, ed. Y. Mellier & G. Meylan, 297–303
 Eigenbrod, A., Courbin, F., Vuissoz, C., et al. 2005, A&A, 436, 25
 Freedman, W. L. 2017, Nature Astronomy, 1, 0121
 Freedman, W. L., Madore, B. F., Gibson, B. K., et al. 2001, ApJ, 553, 47
 Hilbert, S., Hartlap, J., White, S. D. M., & Schneider, P. 2009, A&A, 499, 31
 Jee, I., Komatsu, E., & Suyu, S. H. 2015, J. Cosmology Astropart. Phys., 11, 033
 Liao, K., Treu, T., Marshall, P., et al. 2015, ApJ, 800, 11
 Lin, H., Buckley-Geer, E., Agnello, A., et al. 2017, ApJ, 838, L15
 Magain, P., Courbin, F., & Sohy, S. 1998, ApJ, 494, 472
 McCully, C., Keeton, C. R., Wong, K. C., & Zabludoff, A. I. 2014, MNRAS, 443, 3631
 McCully, C., Keeton, C. R., Wong, K. C., & Zabludoff, A. I. 2017, ApJ, 836, 141
 Mosquera, A. M. & Kochanek, C. S. 2011, ApJ, 738, 96
 Mushotzky, R. F., Edelson, R., Baumgartner, W., & Gandhi, P. 2011, ApJ, 743, L12
 Oguri, M. & Marshall, P. J. 2010, MNRAS, 405, 2579
 Ostrovski, F., McMahon, R. G., Connolly, A. J., et al. 2017, MNRAS, 465, 4325
 Planck Collaboration, Ade, P. A. R., Aghanim, N., et al. 2016, A&A, 594, A13
 Rathna Kumar, S., Tewes, M., Stalin, C. S., et al. 2013, A&A, 557, A44
 Refsdal, S. 1964, MNRAS, 128, 307
 Riess, A. G., Macri, L. M., Hoffmann, S. L., et al. 2016, ApJ, 826, 56
 Rusu, C. E., Fassnacht, C. D., Sluse, D., et al. 2017, MNRAS, 467, 4220
 Sluse, D., Sonnenfeld, A., Rumbaugh, N., et al. 2016, ArXiv1607.00382
 Suyu, S. H., Bonvin, V., Courbin, F., et al. 2017, MNRAS, 468, 2590
 Suyu, S. H., Marshall, P. J., Auger, M. W., et al. 2010, ApJ, 711, 201
 Suyu, S. H., Marshall, P. J., Blandford, R. D., et al. 2009, ApJ, 691, 277
 Suyu, S. H., Marshall, P. J., Hobson, M. P., & Blandford, R. D. 2006, MNRAS, 371, 983
 Suyu, S. H., Treu, T., Hilbert, S., et al. 2014, ApJ, 788, L35
 Tewes, M., Courbin, F., & Meylan, G. 2013a, A&A, 553, A120
 Tewes, M., Courbin, F., Meylan, G., et al. 2013b, A&A, 556, A22
 Treu, T. & Koopmans, L. V. E. 2002, MNRAS, 337, L6
 Vuissoz, C., Courbin, F., Sluse, D., et al. 2008, A&A, 488, 481
 Wong, K. C., Suyu, S. H., Auger, M. W., et al. 2017, MNRAS, 465, 4895

- ¹ Institute of Physics, Laboratory of Astrophysics, Ecole Polytechnique Fédérale de Lausanne (EPFL), Observatoire de Sauverny, 1290 Versoix, Switzerland
- ² Fermi National Accelerator Laboratory, P.O. Box 500, Batavia, IL 60510, USA
- ³ Department of Physics, University of California, Davis, CA 95616, USA
- ⁴ Kavli Institute for Cosmological Physics, University of Chicago, Chicago, IL 60637, USA
- ⁵ Kavli Institute for Particle Astrophysics and Cosmology, Stanford University, 452 Lomita Mall, Stanford, CA 94035, USA
- ⁶ Max Planck Institute for Astrophysics, Karl-Schwarzschild-Strasse 1, D-85740 Garching, Germany
- ⁷ Physik-Department, Technische Universität München, James-Franck-Straße 1, 85748 Garching, Germany
- ⁸ Institute of Astronomy and Astrophysics, Academia Sinica, P.O. Box 23-141, Taipei 10617, Taiwan
- ⁹ Department of Physics and Astronomy, University of California, Los Angeles, CA 90095, USA
- ¹⁰ Departamento de Ciencias Físicas, Universidad Andres Bello Fernandez Concha 700, Las Condes, Santiago, Chile
- ¹¹ Millennium Institute of Astrophysics, Chile
- ¹² Instituto de Física y Astronomía, Universidad de Valparaíso, Avda. Gran Bretaña 1111, Playa Ancha, Valparaíso 2360102, Chile
- ¹³ Argelander-Institut für Astronomie, Auf dem Hügel 71, 53121, Bonn, Germany
- ¹⁴ European Southern Observatory, Karl-Schwarzschild-Strasse 2, D-85748 Garching bei Munchen, Germany
- ¹⁵ Centro de Astroingeniería, Facultad de Física, Pontificia Universidad Católica de Chile, Av. Vicuña Mackenna 4860, Macul 7820436, Santiago, Chile
- ¹⁶ Max-Planck-Institut für Astronomie, Königstuhl 17, 69117 Heidelberg, Germany
- ¹⁷ Cerro Tololo Inter-American Observatory, National Optical Astronomy Observatory, Casilla 603, La Serena, Chile
- ¹⁸ Institute of Astronomy, University of Cambridge, Madingley Road, Cambridge CB3 0HA, UK
- ¹⁹ Kavli Institute for Cosmology, University of Cambridge, Madingley Road, Cambridge CB3 0HA, UK
- ²⁰ LSST, 933 North Cherry Avenue, Tucson, AZ 85721, USA
- ²¹ CNRS, UMR 7095, Institut d’Astrophysique de Paris, F-75014, Paris, France
- ²² Department of Physics & Astronomy, University College London, Gower Street, London, WC1E 6BT, UK
- ²³ Sorbonne Universités, UPMC Univ Paris 06, UMR 7095, Institut d’Astrophysique de Paris, F-75014, Paris, France
- ²⁴ Kavli Institute for Particle Astrophysics & Cosmology, P. O. Box 2450, Stanford University, Stanford, CA 94305, USA
- ²⁵ SLAC National Accelerator Laboratory, Menlo Park, CA 94025, USA
- ²⁶ Laboratório Interinstitucional de e-Astronomia - LIneA, Rua Gal. José Cristino 77, Rio de Janeiro, RJ - 20921-400, Brazil
- ²⁷ Observatório Nacional, Rua Gal. José Cristino 77, Rio de Janeiro, RJ - 20921-400, Brazil
- ²⁸ Department of Astronomy, University of Illinois, 1002 W. Green Street, Urbana, IL 61801, USA
- ²⁹ National Center for Supercomputing Applications, 1205 West Clark St., Urbana, IL 61801, USA
- ³⁰ Institut de Física d’Altes Energies (IFAE), The Barcelona Institute of Science and Technology, Campus UAB, 08193 Bellaterra (Barcelona) Spain
- ³¹ Department of Physics and Astronomy, University of Pennsylvania, Philadelphia, PA 19104, USA
- ³² George P. and Cynthia Woods Mitchell Institute for Fundamental Physics and Astronomy, and Department of Physics and Astronomy, Texas A&M University, College Station, TX 77843, USA
- ³³ Department of Physics, IIT Hyderabad, Kandi, Telangana 502285, India
- ³⁴ Institut de Ciències de l’Espai, IEEC-CSIC, Campus UAB, Carrer de Can Magrans, s/n, 08193 Bellaterra, Barcelona, Spain
- ³⁵ Instituto de Física Teórica UAM/CSIC, Universidad Autonoma de Madrid, 28049 Madrid, Spain
- ³⁶ Department of Astronomy, University of California, Berkeley, 501 Campbell Hall, Berkeley, CA 94720, USA
- ³⁷ Lawrence Berkeley National Laboratory, 1 Cyclotron Road, Berkeley, CA 94720, USA
- ³⁸ Center for Cosmology and Astro-Particle Physics, The Ohio State University, Columbus, OH 43210, USA
- ³⁹ Department of Physics, The Ohio State University, Columbus, OH 43210, USA
- ⁴⁰ Astronomy Department, University of Washington, Box 351580, Seattle, WA 98195, USA
- ⁴¹ Australian Astronomical Observatory, North Ryde, NSW 2113, Australia
- ⁴² Argonne National Laboratory, 9700 South Cass Avenue, Lemont, IL 60439, USA
- ⁴³ Departamento de Física Matemática, Instituto de Física, Universidade de São Paulo, CP 66318, São Paulo, SP, 05314-970, Brazil
- ⁴⁴ Institució Catalana de Recerca i Estudis Avançats, E-08010 Barcelona, Spain
- ⁴⁵ Jet Propulsion Laboratory, California Institute of Technology, 4800 Oak Grove Dr., Pasadena, CA 91109, USA
- ⁴⁶ Centro de Investigaciones Energéticas, Medioambientales y Tecnológicas (CIEMAT), Madrid, Spain
- ⁴⁷ Department of Physics, University of Michigan, Ann Arbor, MI 48109, USA
- ⁴⁸ School of Physics and Astronomy, University of Southampton, Southampton, SO17 1BJ, UK
- ⁴⁹ Instituto de Física Gleb Wataghin, Universidade Estadual de Campinas, 13083-859, Campinas, SP, Brazil
- ⁵⁰ Computer Science and Mathematics Division, Oak Ridge National Laboratory, Oak Ridge, TN 37831